Abstract There has been an increasing interest in photonic generation of RF signals in the millimeter-wave (30 GHz ∼ 300 GHz) and/or terahertz-wave (0.1 THz ∼ 10 THz) regions, and photodiodes play a key role in it. This paper reviews recent progress in the high-power RF photodiodes such as Uni-Traveling-Carrier-Photodiodes (UTC-PDs), which operate at these frequencies. Several approaches to increasing both the bandwidth and output power of photodiodes are discussed, and promising applications to broadband wireless communications and spectroscopic sensing are described.

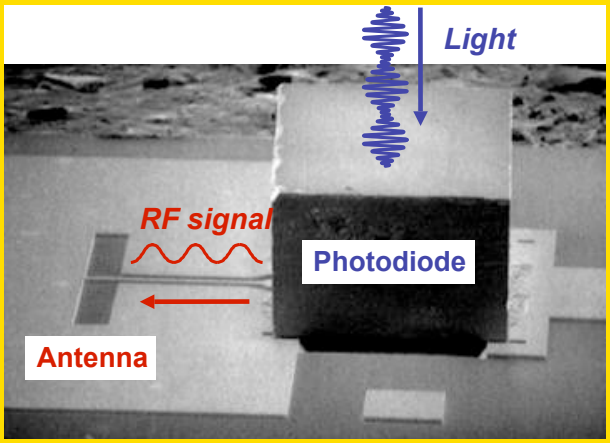

Photodiode chip is bonded to the substrate with the antenna. This is a symbolic figure of RF photonics in this article.

High-power RF photodiodes and their applications

Tadao Nagatsuma[1,2,*], *Hiroshi Ito*[3], *and Tadao Ishibashi*[4]

[1] Graduate School of Engineering Science, Osaka University, 1-3 Machikanemaya, Toyonaka, Osaka 560-8531, Japan
[2] NTT Microsystem Integration Laboratories, 3-1 Morinosato Wakamiya, Atsugi, Kanagawa 243-0198, Japan
[3] Center for Natural Sciences, Kitasato University, 1-15-1 Kitasato, Sagamihara, Kanagawa 228-8555, Japan
[4] NTT Electronics Corporation, 3-1 Morinosato Wakamiya, Atsugi, Kanagawa 243-0198, Japan

Received: 6 June 2008, Revised: 14 July 2008, Accepted: 18 July 2008
Published online: 3 September 2008

Key words: High frequency, high power, photodiode, uni-traveling-carrier photodiode, spectroscopy, wireless link.

PACS: 85.60.Dw, 84.40.-x, 07.57.Hm, 07.57.Pt, 84.40.Ua

1. Introduction

Research on exploring millimeter-waves (MMWs) and terahertz (THz) waves, which cover the frequency range from 30 GHz to 10 THz, has lately become very active, since nature of these electromagnetic waves is suited to spectroscopic sensing [1–3] as well as to ultra-broadband wireless communications [4–6]. One of the obstacles to develop applications of MMWs and THz waves is a lack of solid-sate signal sources, rather than detectors [7], as the frequency band in this region is often referred to as "terahertz gap" [8].

For the generation of MMWs and THz waves, photonic techniques are considered to be superior to conventional techniques based on electronic devices with respect to wide frequency bandwidth, tunability, and stability. Moreover, the use of optical fiber cables enables us to distribute high-frequency RF signals over long distances [9]. In this scheme, optical-to-electrical (O-E) converters, or photodiodes, which operate at long optical wavelengths (1.3–1.55 μm), play a key role, and high-output-current operation is required in addition to high-frequency operation for practical applications. Among various types of long-wavelength photodiode technologies, a uni-traveling-carrier photodiode (UTC-PD) has exhibited the highest output power at frequencies from 100 GHz to 1 THz, with improvement in layer and device structures since its debut in 1997 [10].

In this paper, we review recent progress in the UTC-PDs in comparison with other types of photodiodes, and their applications to wireless communications, radio astronomy, and spectroscopy. In Sect. 2, background and motivation in the photonic generation of MMW and THz-wave signals

* Corresponding author: e-mail: nagatuma@ee.es.osaka-u.ac.jp, ngtm@aecl.ntt.co.jp

are explained. Next, basic properties of high-power photodiodes and their evolution are described in Sects. 3 and 4. Finally, we discuss some of the latest RF applications of such photodiodes to communications and measurements in Sect. 5.

2. Photonic generation of MMW/THz-wave signals

Fig. 1 shows a block diagram of a photonics-based radio-wave transmitter. First, the optical signal, whose amplitude or phase is modulated at MMW/THz frequencies, is generated by the optical RF signal source, and is delivered through optical fiber cables, and converted to the electrical signal by a high-frequency O-E converter such as a photodiode. The converted signal is finally radiated into free space by an antenna. In some cases, the output of the photodiode is followed by a power amplifier and/or a frequency multiplier, only when these electronic devices are available at frequencies of interest.

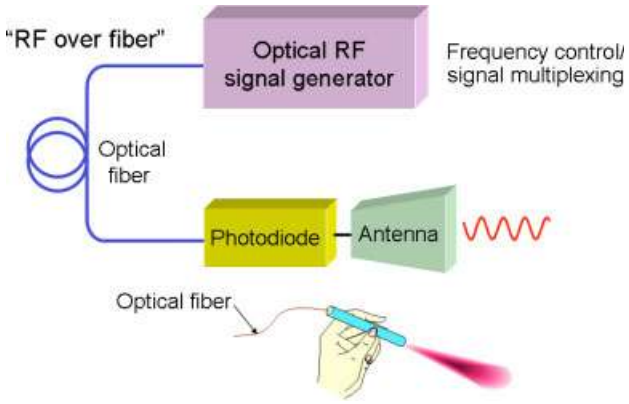

Figure 1 (online color at: www.lpr-journal.org) Conceptual illustration of photonic MMW/THz-wave generators.

As for continuous-wave (CW) optical MMW/THz signal generation, main techniques being currently investigated include optical heterodyning using two different wavelengths light [11], optical injection-locking of a laser diode by a master laser [12], combination of a single-mode laser with an external modulator [13], and actively mode-locked lasers [14, 15]. Among these, the optical heterodyning technique offers the widest frequency tunability from GHz to THz regions. The optical heterodyning using two laser sources such as wavelength-tunable lasers, as shown in Fig. 2a, is the simplest and also a cost-effective way. Here, there is no need to employ expensive electrical devices operating at MMW and/or THz frequencies. The frequency stability, however, is generally poor; for instance, the phase noise is -75 dBc/Hz at an offset frequency of 100 MHz, and the frequency drift is more than 10 MHz/hour, when two DFB lasers are used [16]. Thus, a special phase-locking system is necessary for practical instrumentations.

Fig. 2b shows another optical heterodyning technique which can generate extremely low-phase-noise signals [17–21]. Key components are an optical frequency comb generator (OFCG), which generates multi-frequency (wavelength) optical signals [22–25], and an optical filter, which selects two of these. Typical OFCGs are mode-locked short-pulse lasers, and a combination of a single-mode laser and optical amplitude and/or phase modulators. They generate multi-frequency optical signals with a spacing of the driving frequency, f_0, for lasers or modulators, and all modes are phase-locked. The selection and combination of two modes corresponds to frequency multiplication, Nf_0. The fundamental frequency, f_0, is usually 10 to 30 GHz, where

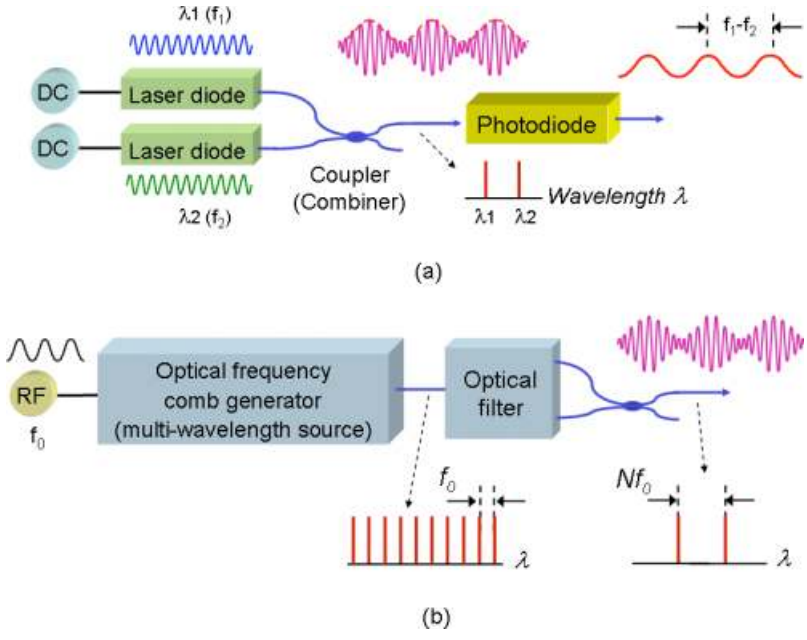

Figure 2 (online color at: www.lpr-journal.org) Block diagram of the MMW/THz-wave generator based on optical heterodyning technique.

optical modulators and driver electronics are commercially available, and the multiplication factor can be made over 50 [22, 25–27]. Since fine and accurate tuning of f_0 is possible by using a synthesized signal generator, we can continuously change the frequency from f_0 to Nf_0. Phase noise of generated signal is N times as large as that of the synthesized signal generator [27].

Thus, the advantage of photonically assisted MMW/THz signal generation is that continuously tunable and low-phase-noise signals are available with relatively low-frequency electronic and photonic components. To make this approach realistic, development of high-frequency/high-power O-E converters, or photodiodes is crucial.

3. Principle and advantage of uni-traveling carrier photodiode

Band diagrams of the UTC-PD and traditional pin PD are schematically shown in Figs. 3a and b, respectively [10, 28, 29]. In the pin PD, the light absorption occurs in the intrinsic (depleted) InGaAs region, and electron-hole pairs are created. In contrast, the active region of the UTC-PD consists of two layers; one is a neutral (undepleted) narrow-gap light absorption layer (p-type InGaAs), and the other is an undoped or lightly n-type doped (depleted) wide-gap carrier collection layer (InP). Electron-hole pairs are created only in the absorption layer, while the carrier collection layer is transparent to the illuminated light at a wavelength of 1.55 μm. Greatly dissimilar carrier transport properties (mobility and drift velocity) between electrons and holes are the key in the discussion below.

In the UTC-PD, the photo-generated minority electrons in the absorption layer diffuse and/or drift into the depleted carrier collection layer. When we introduce a quasi-field in the absorption layer by the band-gap grading or doping grading, the traveling time of electrons in the absorption layer can be effectively reduced. Meanwhile, photo-generated majority holes respond very quickly within in the dielectric relaxation time by their collective motion. Hence, the photoresponse of the UTC-PD is dominated by the electron transport in the whole structure. This is an essential difference from the conventional pin PD, where both electrons and holes contribute to the response, and the low-velocity hole-transport dominates the performance. The velocity of electrons ($3–5\times10^7$ cm/s) is 6–10 times higher than that of holes (5×10^6 cm/s). In the UTC-PD, electrons exhibit velocity overshoot in the InP carrier collection layer. We usually set the bias voltage of the UTC-PD to the optimum condition so that electrons can travel at velocity overshoot for a very limited electric field strength [30, 31]. As a result, electron diffusion time in the undepleted region mainly determines the operation speed of the UTC-PD with a moderate absorption layer thickness.

Typical measured pulse responses of the UTC-PD and the pin PD are shown in Figs. 4a and b, respectively [28, 29]. The absorption and collection layers are 220 and 300-nm thick, respectively, for the UTC-PD, and the absorption layer of the pin PD is 300-nm thick. The output waveforms differ greatly from each other. Two current components are observed in the waveforms of pin PD. The initial sharp peak comes from the electron current in the depletion layer. Current tails observed after the peak, however, are due to the slow response of holes. 3-dB bandwidth of the pin PD is dominantly determined by these tails, which are significant for higher optical input energy. To the contrary, the waveforms of UTC-PD are almost symmetry, showing fast falling edges even for higher optical inputs. It must be noted that the fall time of the UTC-PD can be further decreased by shrinking the absorption layer while keeping the collection layer relatively thick [30].

In addition, the RC time constant is another factor which determines the operation speed. The RC limited bandwidth, $f_{3\,\mathrm{dB}}$, is given by $f_{3\,\mathrm{dB}} = 1/RC = d/\varepsilon AR$, where d is a thickness of the active layer, and A is device area. The very thin absorption layer is used to obtain larger transit-time limited bandwidth, but this causes the decrease in the RC limited bandwidth in the pin PD. On the other hand, we can independently design the absorption layer and carrier collection layer thicknesses, thus making the absorption layer thinner to increase the transit-time limited

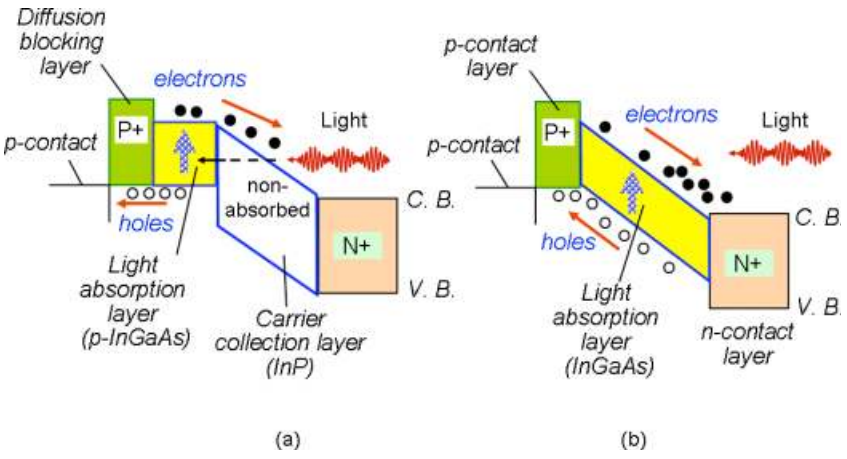

Figure 3 (online color at: www.lpr-journal.org) Band diagram of (a) UTC-PD and (b) pin PD.

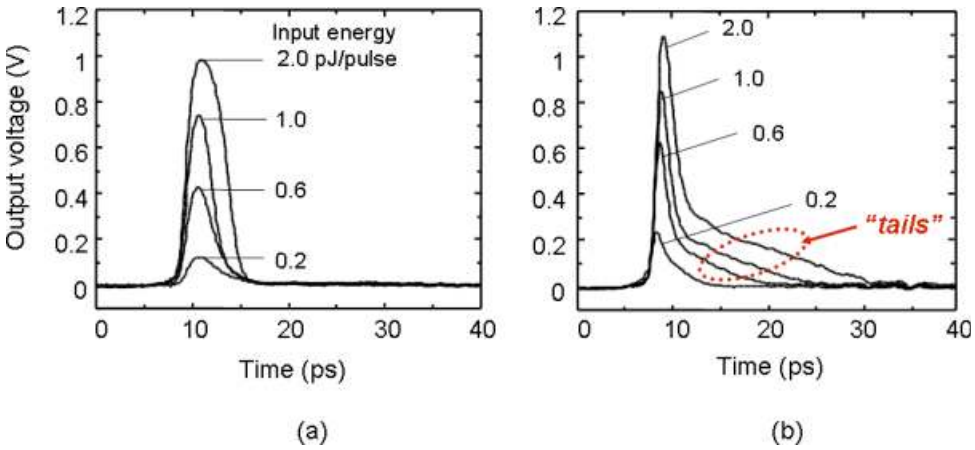

Figure 4 (online color at: www.lpr-journal.org) Pulse photoresponse of (a) UTC-PD and (b) pin PD.

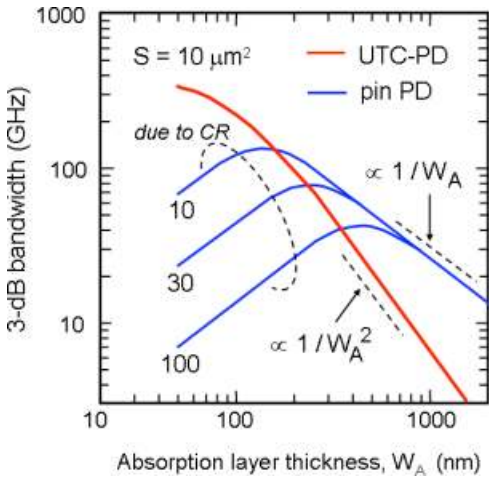

Figure 5 (online color at: www.lpr-journal.org) Relationship between 3 dB-bandwith and the thickness of absorption layer for UTC-PDs and pin PDs.

bandwidth without scarifying the RC charging time in the UTC-PD. An example of calculated 3-dB bandwidth vs. thickness of the absorption layer, W_A, for the UTC-PD and the pin PD is shown in Fig. 5. For thinner absorption layer, the 3-dB bandwidth increases with the inverse of the square of W_A for the UTC-PD and with the inverse of W_A for the pin PD. This difference comes from the difference in the type of carrier transport in the absorption layer; that is, electron transport in the absorption layer is diffusive in the UTC-PD, while the drift motion of both types of carriers is dominant in the conventional pin PD. For much thinner absorption layer, the 3-dB bandwidth turns to decrease due to the increase in the RC time constant in the pin PD, and this is not the case for the UTC-PD.

Another advantage of the UTC-PD is the higher output saturation current even in the high-frequency operation due to much less space charge effect in the depletion layer, which also results from the high electron velocity in the depletion layer. Figs. 6a and b show the mechanism of the space charge effect in the UTC-PD and the conventional pin PD, respectively. The substantial difference in the mechanism leads to an orders-of-magnitude difference in the saturation current. In the pin PD, the band profile is modulated (band bending) under high-excitation condition, since photogenerated carriers are stored in the absorption layer as shown in Fig. 6b. The decreased electric field drastically reduces the carrier velocity, enhances the charge storage, and results in the output current saturation. The situation is similar in the UTC-PD, but the space charge consists of only electrons whose velocity at overshoot is much higher than that of holes even for the decreased electric field. Therefore, the output current does not saturate until the current density becomes an order of magnitude higher than that for the pin PD.

It must be added that similar structures existed prior to the first demonstration of the high-speed/high output-current UTC-PD. Davis et al. [32] reported a photodiode with a 3-μm-thick undepleted InGaAs absorber and a 5-μm-thick InP depletion layer that was designed to decouple the device capacitance (bandwidth) and the optical responsivity (efficiency).

4. Evolution of high-power MMW/THz photodiode technologies

In this section, we discuss the evolution of the UTC-PDs in comparison with recent progress in other types of MMW/THz photodiodes. In Fig. 7, several techniques or approaches are summarized to improve the performance with respect to efficiency (responsivity), bandwidth, output power, and other special items.

4.1. Structure design

In general, there are several approaches in terms of photoabsorption structures [33]. Fig. 8 depicts (a) original surface illuminated PD and (b–d) edge illuminated PDs. The

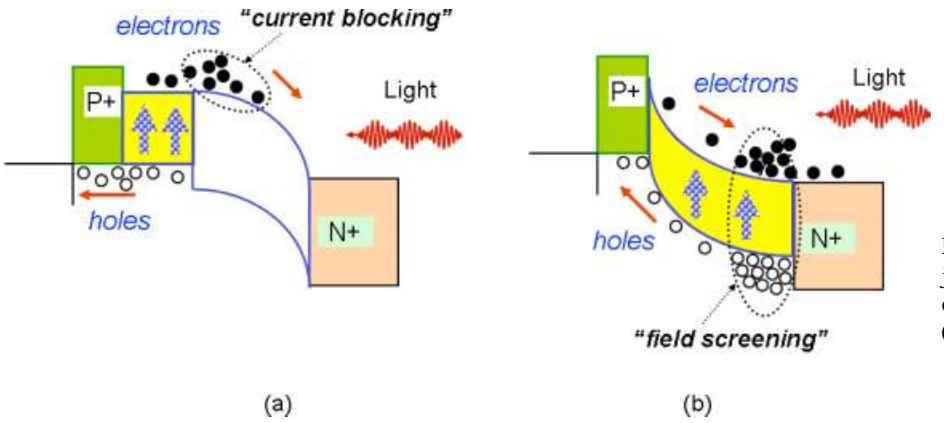

Figure 6 (online color at: www.lpr-journal.org) Modification of band diagram at high-optical input for (a) UTC-PD and (b) pin PD.

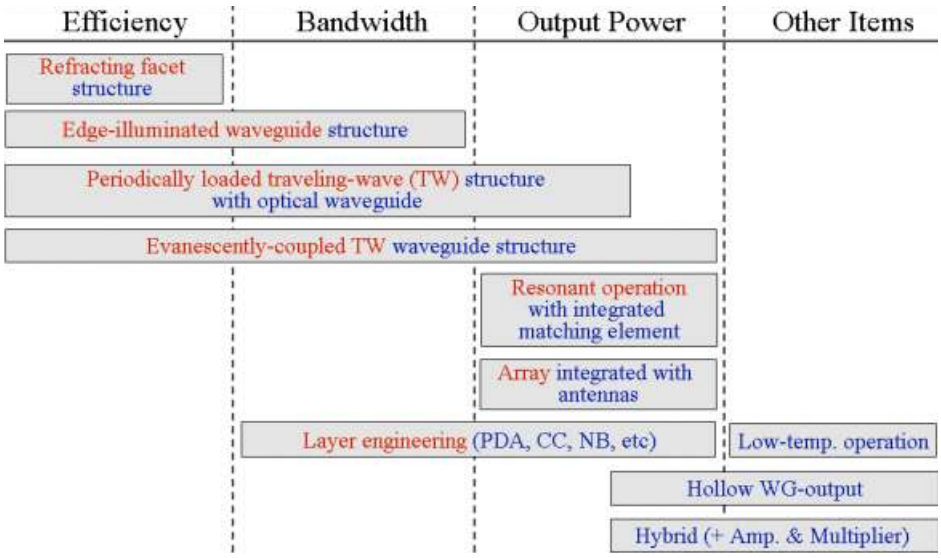

Figure 7 (online color at: www.lpr-journal.org) Technology mapping for the performance evolution of UTC-PDs.

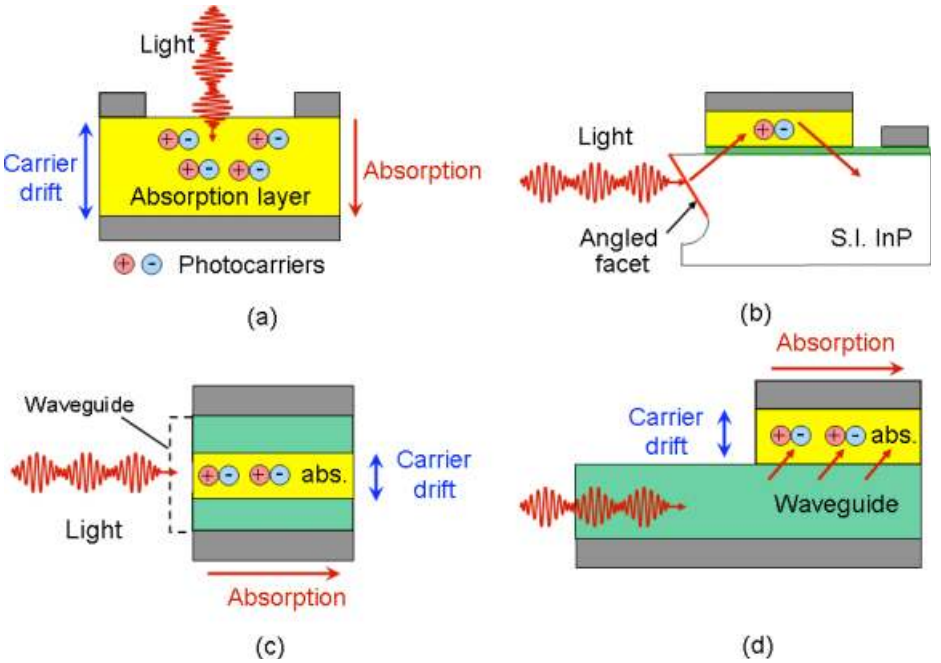

Figure 8 (online color at: www.lpr-journal.org) Structures of photodiodes for (a) surface (vertical) illumination and (b–d) edge (horizontal) illumination. (b) Refracting facet (RF) PD. (c) Waveguide (WG) PD. (d) Waveguide-fed evanescently coupled PD.

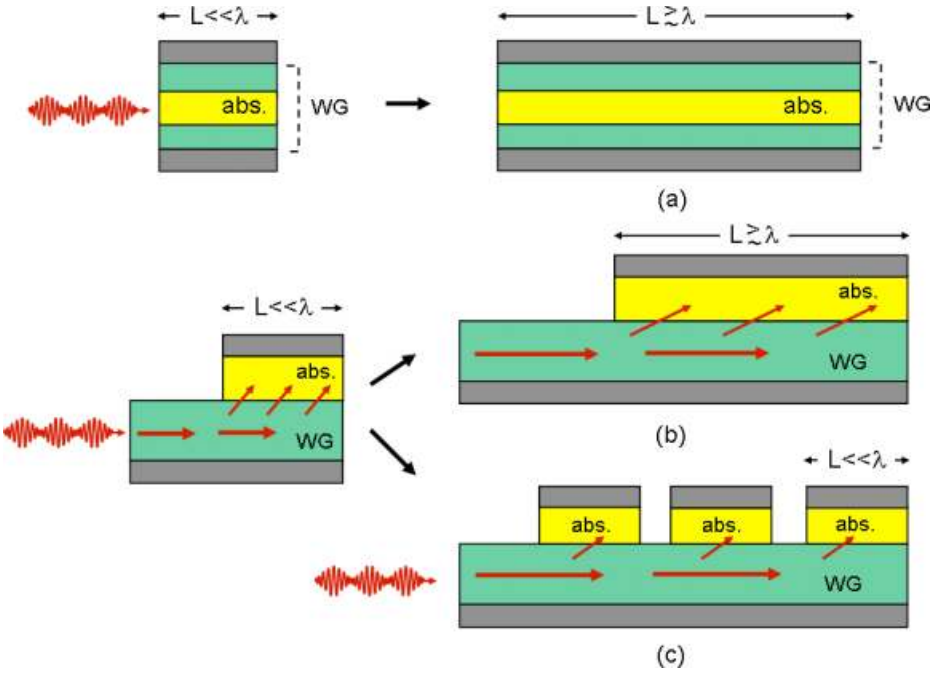

Figure 9 (online color at: www.lpr-journal.org) Distributed structures. (a,b) Traveling-wave PDs. (c) Periodically-loaded traveling-wave PD.

edge-illuminated structures were devised to enhance the responsivity (efficiency) of the PD with maintaining the bandwidth, and they are divided into (b) refracting facet illuminated PD [34], (c) waveguide (WG) structure PD [35], and (d) waveguide-fed evanescently-coupled PD [36]. Moreover, the WG structure PD and waveguide-fed evanescently-coupled PD are extended to distributed structures to further enhance the bandwidth by overcoming RC time constant with increased length of PD in the direction of light illumination as shown in Fig. 9. Distributed structures are divided into (a) (b) traveling-wave PDs [37, 38], and (c) periodically loaded traveling-wave (or velocity-matched distributed) PD [39].

The absorption layer of the WG structure PD acts as a part of core layer for the light waveguide. In the surface or backside illuminated PD, there is a tradeoff between the bandwidth and the efficiency. This is because thin absorption layer enhances carrier-transit-time limited bandwidth, but it decreases the amount of light absorption. On the other hand, speed and efficiency can be independently optimized in the case of edge-illuminated PDs. Fukano et al. first introduced the refracting facet structure in the UTC-PD to enable the edge illumination [40]. Angled (∼55 degree) incident facet was made by anisotropic chemical etching. A responsivity of 1 A/W was obtained at 40 GHz. It also contributes to the ease of packaging, and is effective especially for the tolerant optical alignment. Muramoto et al. introduced the WG structure in the UTC-PD and the measured efficiency reached 50 % with a bandwidth of 55 GHz [41].

By separating the light waveguide layer and the absorption layer, the waveguide-fed evanescently-coupled PD offers more relaxed design optimization to enhance the output power in addition to the efficiency and the bandwidth. Hirota et al. reported the first periodically-loaded TW UTC-PD. A responsivity of 0.05 A/W of the lumped UTC-PD was increased to 0.15 A/W with 9-dB increase in the response by the periodic TW UTC-structure [42]. They also indicated the importance of a termination resistor for the distributed operation at frequencies of > 100 GHz. Recently, there have been increasing reports on waveguide-fed evanescently-coupled TW UTC-PDs theoretically as well as experimentally [43–45].

4.2. Circuit design

Integration of the UTC-PD with passive circuit elements such as stubs and antennas is effective to increase the output power generated from the "lumped" PD. This approach is based on the band-operation of the PD at designated frequencies.

Fig. 10 shows the UTC-PD integrated with a short-stub matching circuit consisting of a CPW and a MIM capacitor [46]. This technique compensates for the internal capacitance of the PD, thus eliminating the constraint of RC time constant at a specific frequency, and increases the output power by more than 3 dB at the resonant frequency. The maximum output power exceeds 20 mW at around 100 GHz for circuit (a) [46], and $> 100\,\mu$W at around 300 GHz for circuit (c) [47].

Integration of a resonant planar antenna with the UTC-PD is also effective in particular for THz regions [44,48,49]. In Fig. 11, an impedance matching was performed between the twin-dipole antenna and the UTC-PD [49]. Generated power exceeds 10 μW at 1 THz.

Fig. 12 shows a comparison of reported MMW/terahertz wave output (or detected) power against operation frequency for UTC-PDs, pin PDs, and low-temperature-grown (LT)-GaAs photomixers. The output power of UTC-PDs is about two orders of magnitude higher than those of pin

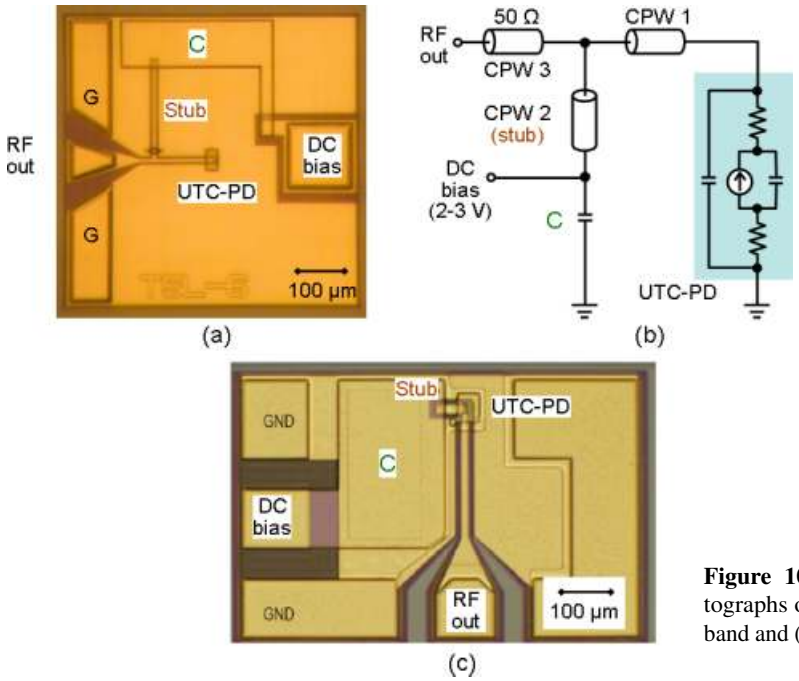

Figure 10 (online color at: www.lpr-journal.org) Photographs of matching-circuit-integrated UTC-PDs for (a) W-band and (c) J-band operation. (b) Simplified equivalent circuit.

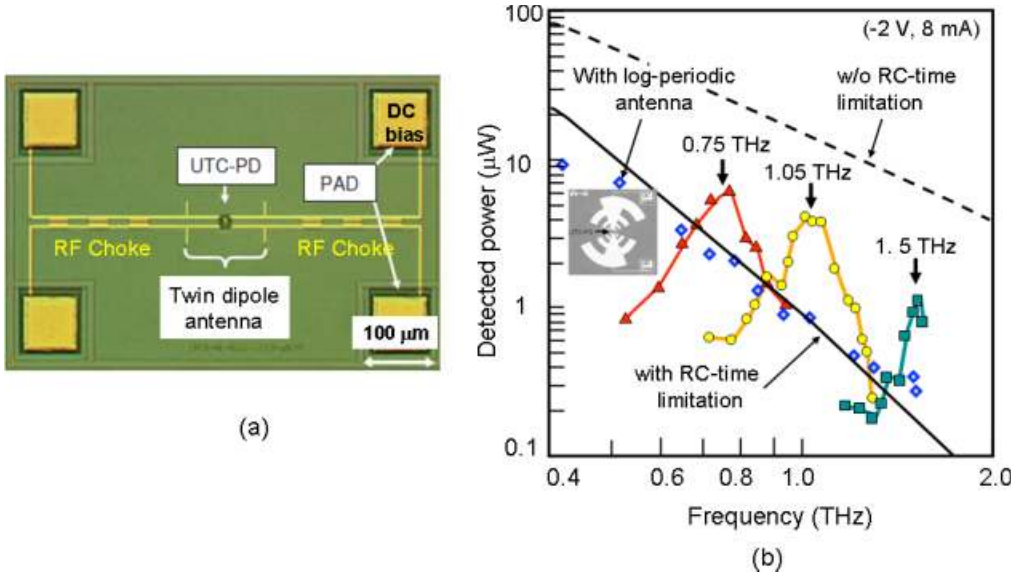

Figure 11 (online color at: www.lpr-journal.org) (a) Photograph of THz UTC-PD chip integrated with twin-dipole antenna. (b) Detected output powers for different designated operation frequencies.

PDs, mostly due to high saturation output current. The output power decreases in proportion to f^{-4}. Recently, UTC-PDs with waveguide-coupled and traveling-wave structure have been reported from a group of University College London [44], which exhibit world-record output power. It must be noted that the output-power measurement of our UTC-PDs was conducted at room temperature with no special heat sinking.

To overcome the limitation of the power capacity in a single device, the power combining technique by using an array of antennas integrated with UTC-PDs was examined [50]. Total output power of 1 mW is expected for 3×3 array at 300 GHz.

4.3. Carrier transport design

There is still a room for the optimization of layer structures and materials by considering the carrier dynamics in the PD [51,52]. In Fig. 13, we summarize diode layer structures which have been examined so far to improve performance parameters in terms of speed (bandwidth), efficiency (responsivity) and output power (saturation current), starting from conventional pin PD (a) and UTC-PD (b), though this classification does not cover completely all the layer structures reported. Strict tradeoff exists between theses parameters, and the constraints depend on the diode layer structure. It should also be noted that the device scaling

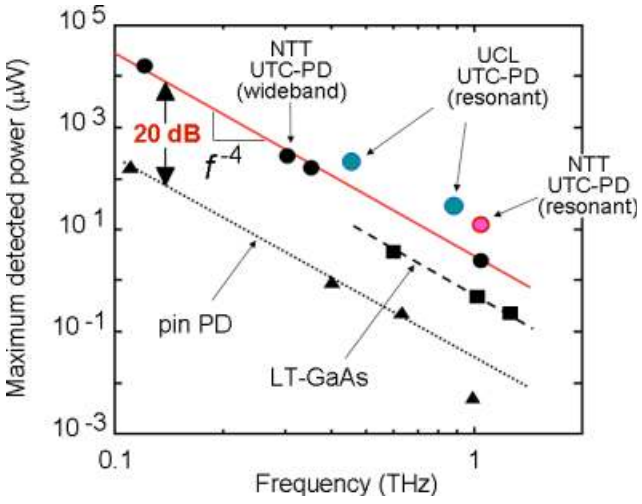

Figure 12 (online color at: www.lpr-journal.org) Comparison of reported MMW/THz output power against operation frequency for UTC-PD, pin PD and LT-GaAs photomixer.

can always increase the bandwidth. So, the comparison has to be done under some conditions. Here, all the structures are supposed to have same junction size and capacitance, thus, the RC time constant and self heating are common. As described in Sect. 3, the UTC-PD (b) gets rid of hole transport in its operation, which is a cause of slow response and low saturation level in the pin PD (a). Also in other structures (c,d), space-charge generation by hole transport can be minimized to relax the field modulation.

Dual (depleted and undepleted) absorbers are used in Fig. 13c, and this type is often referred to as partially-doped absorber (PDA) PD [53–56]. The PDA-PD is essentially equivalent to the InP/InGaAs UTC-PD with an InP collector replaced by an InGaAs collector. This structure operates with lower hole density than the pin PD and its saturation level becomes higher. Thinner InGaAs depletion layer in the PDA-PD compared to that in the pin PD is substantial in terms of thermal management, since thermal conductivity of InGaAs is poor. This structure is also effective to increase the responsivity. Muramoto et al. [54] demonstrated that a responsivity of 0.98 A/W was achieved with a photocurrent of 10 mA at 50 GHz, and Li et al. [55] reported 0.6 A/W with a saturation current of 24 mA at 48 GHz.

Hybrid pin-like structure shown in Fig. 13d, where absorbed and non-absorbed intrinsic layers are combined, is referred to as dual depletion pin PD [57, 58]. Williams [57] compared the performance of dual depletion pin PD with conventional pin PD and UTC-PD based on space-charge and thermal calculations.

The layer structure shown in Fig. 13e is a composite of the UTC-PD and the dual depletion pin PD. The thickness of the depleted InGaAs can be minimized for a condition of equal total InGaAs thickness. This results in considerably less hole space-charge density and higher output

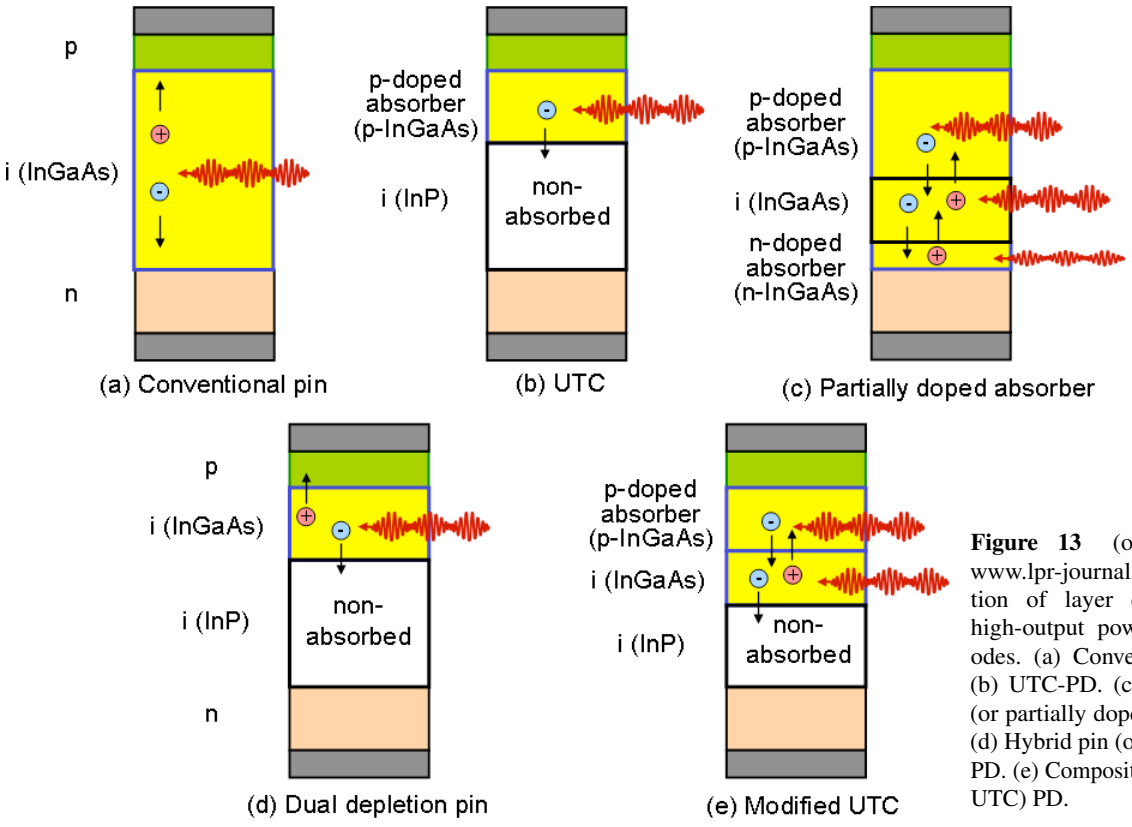

Figure 13 (online color at: www.lpr-journal.org) Classification of layer engineering for high-output power RF photodiodes. (a) Conventional pin PD. (b) UTC-PD. (c) Dual absorber (or partially doped absorber) PD. (d) Hybrid pin (or dual depletion) PD. (e) Composite-type (modified UTC) PD.

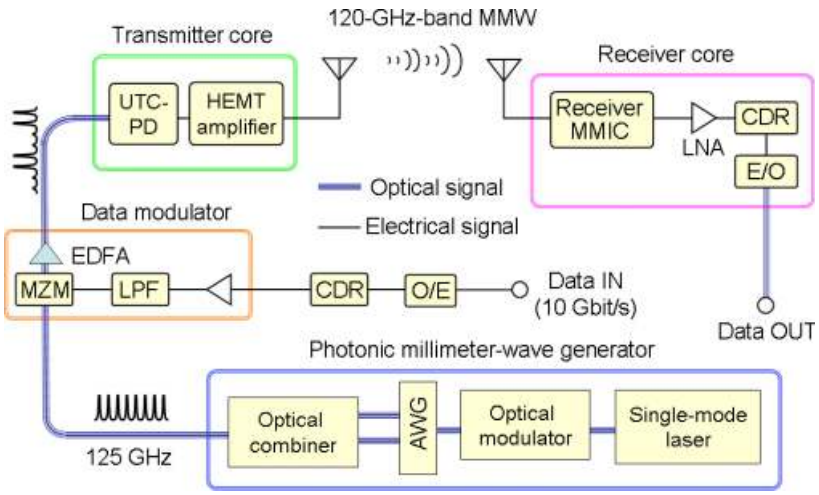

Figure 14 (online color at: www.lpr-journal.org) Schematic diagram of the wireless link systems using photonics-based MMW transmitter.

saturation level. This PD is sometimes labeled as modified UTC-PD [59]. We also notice that the composite structure includes all design elements and others are variations of this structure.

In the UTC and UTC-like structures Fig. 13b,d,e, the i-InP carrier collection layer can be replaced with a doped-InP in order to avoid the space charge effect, and to accelerate electrons by near-ballistic (NB) transport behavior [60, 61]. The former is sometimes called as charge-compensated (CC) structure [62].

4.4. Other engineering challenges

One of the remaining practical issues in the high-power UTC- and UTC-like PDs is a thermal management. These photodiodes often face burn out before their saturation condition due to thermal effect. To transfer heat out of the photodiode effectively, use of Si substrate by wafer (epi-layer) bonding [63, 64], and metal to metal (heat spreader) bonding [65] has been examined.

Ultra-low temperature operation of the UTC-PD is attractive, since it can be integrated with superconducting mixers and other quantum-effect electron devices operating at low temperature (4–77 K). Due to the wavelength dependence of the responsivity of the UTC-PD at low temperatures, a smaller bandgap absorption layer will be necessary at 1.55 μm [66, 67].

For application to some practical instruments, it is often desirable to deliver the output power to the rectangular waveguide rather than a free-space. W-band (75–110 GHz), F-band (90–140 GHz), D-band (110–170 GHz), and J-band (220–325 GHz) PD modules with rectangular (hollow) waveguides were developed [47,68]. The waveguide-output module can be easily combined with other active components with hollow-waveguide I/O ports such as power amplifiers and frequency multipliers. Using the W-band PD module, the power amplifier, and the multiplier (2×3), the output power of 500 μW was obtained at 500 GHz [69].

5. MMW/THz applications of high-power photodiodes

5.1. High-speed wireless communications

One of common concerns when we use > 100-GHz radio waves for wireless communications is a large propagation loss in the air. From 100 to 300 GHz, there are three valleys, where the attenuation is a local minimum; 75–100 GHz, 110–150 GHz, and 220–270 GHz. Our initial choice is the 120-GHz band centered at 125 GHz.

A block diagram of a 120-GHz-band wireless link system with 10-Gbit/s transmission capability is shown in Fig. 14 [4, 70–72]. A photonic MMW generator is used in the transmitter. An optical MMW source generates optical subcarrier signals whose intensity is modulated at 125 GHz. An optical intensity (ASK) modulator modulates the optical subcarrier signal using data signals. The modulated subcarrier signal is amplified by an optical amplifier and input to the high-power photodiode. The photodiode converts the optical signals into MMW signals, which are amplified and radiated toward the receiver via an antenna. The received MMW signals are amplified and demodulated by a simple envelope detection scheme, for example. The MMW receiver is composed of all-electronic devices using InP-HEMT technology.

The promising application of the above 10-Gbit/s wireless link is found in the broadcasting industry. A wireless link system that can transmit “uncompressed” high-definition television (HDTV) signals has been strongly desired, because TV program production based on the HDTV standard is spreading rapidly in TV stations due to the launch of digital TV broadcasting all over the world. An uncompressed HDTV signal (HD-SDI: high definition serial digital interface) requires a data rate of 1.5 Gbit/s per channel. Conventionally, for wireless transmission of broadcast materials, a 7- or 10-GHz-band microwave field pick-up unit (FPU) is used. The data rate of the state-of-the-art FPUs is as low as 3–80 Mbit/s, which cannot handle the

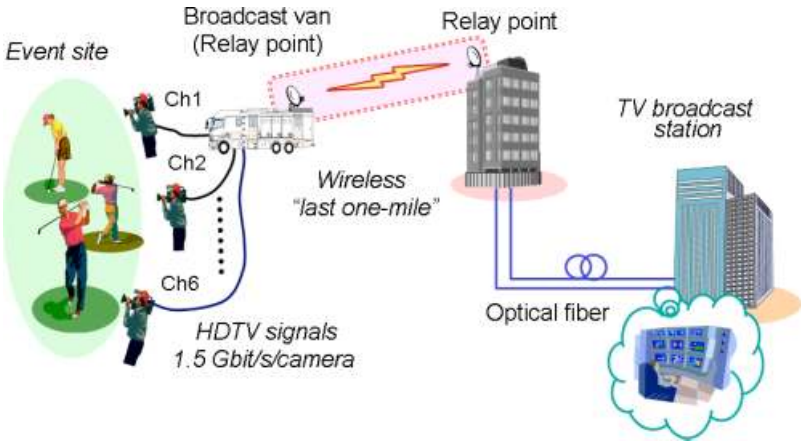

Figure 15 (online color at: www.lpr-journal.org) Application scene of the 10-Gbit/s wireless link system.

full bandwidth of real-time HD-SDI signals. Therefore, current microwave wireless link compresses the HD-SDI signals with MPEG or JPEG2000 encoders. This compression always causes a time delay, which makes it difficult to edit programs or switch cameras in a live broadcast, and sometimes causes deterioration of HD-SDI signal quality. MMWs are suitable for increasing the data rate of wireless communications systems, because the data rate generally increases with the carrier frequency. Commercial wireless links using 60-GHz-band MMWs have a data rate of over 1.5 Gbit/s and thus a capability of transmitting one channel of uncompressed HD-SDI signals. However, large-scale live relay broadcasts, such as golf tournaments and music concerts, requires multiple channels of uncompressed HD-SDI signals. The 120-GHz-band system allows up to 6 channels of HDTV material to be sent over a wireless link with no latency.

For such a purpose, this link uses a high-gain ($\sim$50 dBi) Cassegrain antenna, and can support the optical network standards of both 10 GbE (10.3 Gbit/s) and OC-192 (9.95 Gbit/s) with a bit error rate of 10^{-12}. We have also been successful in the wireless transmission of 6-channel uncompressed high-definition television (HDTV) signals using the link. The 120-GHz-band wireless link will be used in the last-one-mile between a relay van and a broadcast station, where optical fibers cannot be installed easily, as shown in Fig. 15.

One of the advantages of the photonically-assisted MMW transmitter is to make the transmitter core (Fig. 14) very compact and light-weight, so we can bring and place the antenna unit anywhere in the field. The photonic MMW transmitter can be expanded to the multi-band system for reliable and secure data transmission by controlling the center frequency at the site of optical MMW signal generator [73].

In addition, a heterodyne receiver for the 120-GHz-band wireless link has been examined using our photonic MMW generator as a local oscillator (LO), and sufficient stability of the photonic LO has been confirmed [4]. To achieve much higher data rate of >20 Gbit/s, use of 200–300 GHz carrier frequency is promising, and preliminary experiment has been performed with photonically generated 240-GHz waves [74].

5.2. Spectroscopic measurement systems

The ultralow-noise characteristics of the photonically generated MMW/THz-wave signal have been verified through their application to the LO for superconducting (SIS: superconductor-insulator-superconductor) mixers in heterodyne receivers used for radio astronomy. Radio-astronomical signals from the universe have been successfully observed using a 98-GHz photonic LO [75]. Use of the photonic LO in the SIS mixer system is the best combination, since the SIS mixer requires an LO power as low as a few 10 nW, that has been already achieved with the use of RF photodiodes [76]. Another advantage of the photonic LO in spectroscopic measurement systems is their wide tunability. For this purpose, a wideband receiver has been tested with the same combination of the SIS mixers and the photonic LO at frequencies from 260 to 340 GHz [77]. Low-temperature operated UTC-PD [67] will make the photonic LO more attractive for integration with the SIS mixer.

Using the photonic MMW/THz-wave generator, simple spectroscopic measurements has successfully been demonstrated in the frequency range between 240 and 360 GHz [78]. The sample under the test was a mixture of N_2O and N_2 in the ratio of 3:1 (75 %), and filled in a 1-m long gas cell with atmospheric pressure. The experiment setup is shown in Fig. 16. The MMW/THz signal generator was computer controlled to sweep the frequency and the optical MMW/THz signal before the UTC-PD was intensity modulated at a frequency of 10 kHz. Then, the generated signal was radiated and collimated with a diagonal horn antenna and a gold-coated off-axis parabolic mirror, respectively. The transmitted signal through the gas cell was received with a Schottky barrier diode, and detected with a lock-in amplifier tuned at 10 kHz.

The measured transmittance for the gas is plotted in Fig. 17 with simulated results based on the HITRAN database [79]. As can be seen, the positions, tendency of the magnitude and the shape of absorption peaks from the measurement coincide well with those of HITRAN. Measurement bandwidth can be extended by using a photomixer and a receiver, which are integrated with broadband antennas [48, 49, 80].

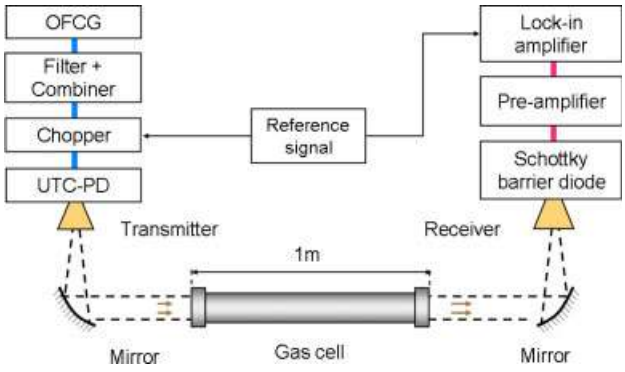

Figure 16 (online color at: www.lpr-journal.org) Experiment setup for spectroscopic measurement system using photonic MMW/THz signal generators.

In the future, this system will be extended to the standoff sensing system for toxic and/or dangerous gasses such as CO, CO_2, HCN, HCl, SO_x, NO_x, etc. in case of disaster or fire (Fig. 18). In this system, highly-sensitive receiver is required, and a heterodyne receiver using the SIS mixer mentioned above is one of the candidates.

6. Future outlook

With recent advent of high-power photodiode technologies, photonically generated MMW/THz waves have proven to be useful in real-world applications such as communications and measurements. In order to expand application fields, the increase of output power by at least one order is desired at higher frequencies. Currently, the maximum available output power at 1 THz is around 10 μW. Fig. 19 summarizes technical points to be examined in order to increase the total power by two orders. In addition to the improvement of photodiode performance in terms of saturation current and thermal management, efficient RF coupling between the photodiode and the antenna is also important. The above countermeasure will allow the single device

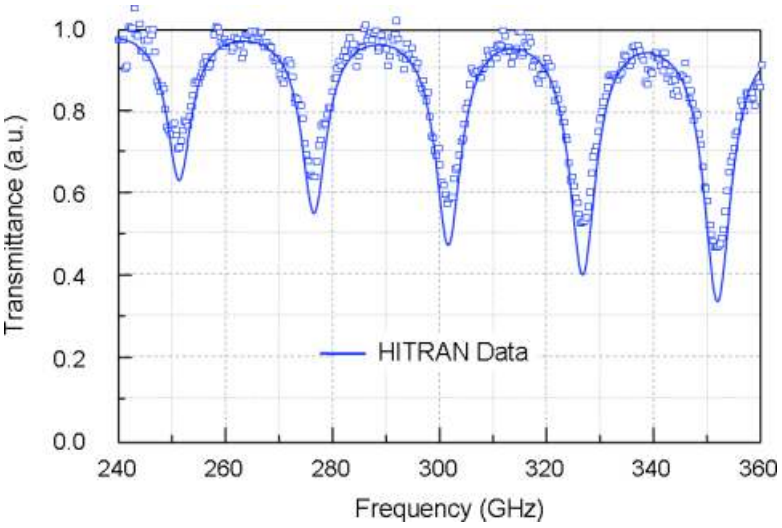

Figure 17 (online color at: www.lpr-journal.org) Measured and simulated spectroscopic results for N_2O concentration of 75%.

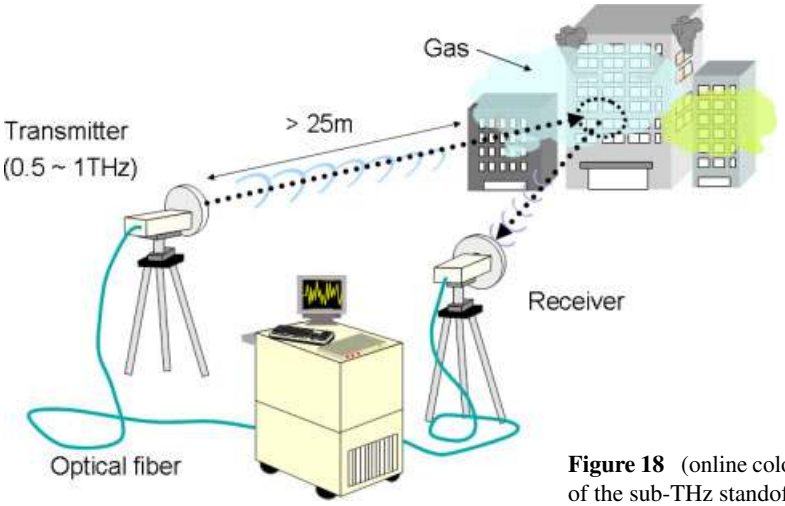

Figure 18 (online color at: www.lpr-journal.org) Targeted application scene of the sub-THz standoff gas sensing system.

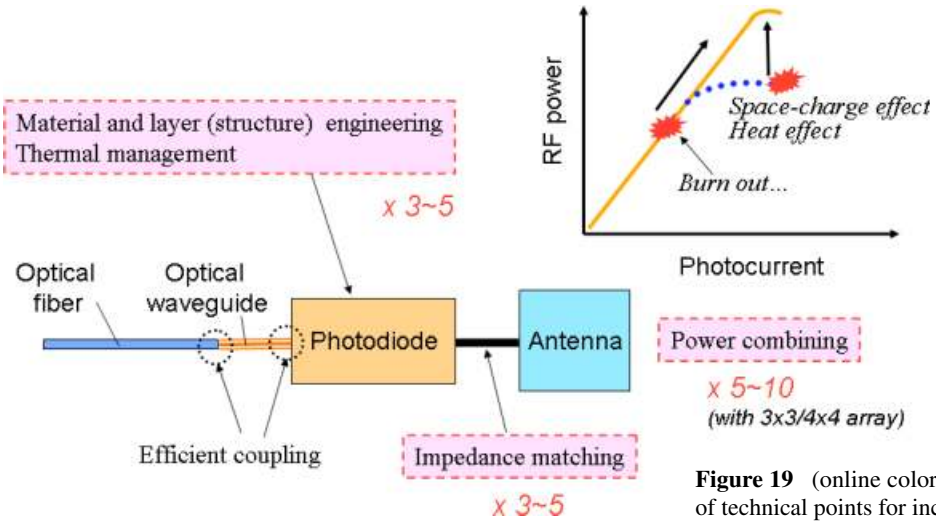

Figure 19 (online color at: www.lpr-journal.org) Summary of technical points for increasing the output power.

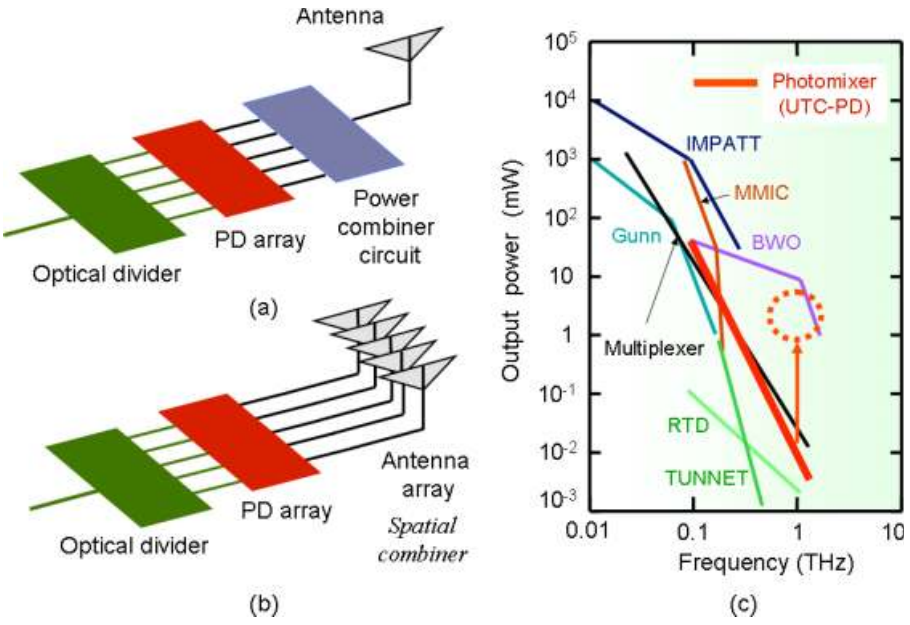

Figure 20 (online color at: www.lpr-journal.org) (a,b) Schematic figures of power-combining techniques. (c) Present and future target of output power from UTC-PDs.

to emit powers on the level of 100 μW at 1 THz [81]. The power combining technique using an array of PDs is promising to increase the output power up to 1-mW level. As shown in Fig. 20, there are two ways of power combining; one uses an electrical power combiner circuit (a), and the other is based on spatial power combination using an array of antennas (b). We believe that these series of challenges will lead to the change in the position of photonics-based THz signal generator (photomixer) as shown in Fig. 20c in the terahertz gap.

Acknowledgements The authors wish to thank Drs. Y. Kado, N. Kukutsu, A. Hirata, R. Yamaguchi, H. Takahashi, H. Togo, N. Shimizu, H.-J. Song, K. Ajito, T. Kimura, T. Furuta, A. Wakatsuki, R. Takahashi, T. Kosugi, K. Murata, K. Iwatsuki, H. Suzuki, and M. Fujiwara for their contribution and support. Part of this work was supported by the "Research and Development Project for the Expansion of Radio Spectrum Resources" made available by the Ministry of Internal Affairs and Communications, Japan, the National Institute of Communications Technology, Japan, and the Ministry of Education, Science, Sports and Culture, Grant-in-Aid for Scientific Research (A), 20246062, 2008.

Tadao Nagatsuma, born in 1958, studied electronics and received his Ph. D. on superconducting devices at Kyushu University (Fukuoka, Japan). Since joining NTT Laboratories, he has worked on high-frequency devices and their application to communications, measurements and sensing. Now, he holds a position of professor at Osaka University.

Hiroshi Ito studied physics at Hokkaido University (Sapporo, Japan), and joined NTT Laboratories in 1982. He achieved his Ph. D. on carrier transport in high speed electron devices. He has been working on compound semiconductors and their applications to ultrafast electron and opto-electronic devices. Currently, he is a professor of Kitasato University.

Tadao Ishibashi, born in 1949, studied applied physics at Hokkaido University (Sapporo, Japan). Since joining NTT Laboratories, he has worked on high-speed III-V and optoelectronic devices. Now, he is a senior engineer at Photonic Technology Development Center of NTT Electronics.

References

[1] W. L. Chan, J. Deibel, and D. Mittleman, Imaging with terahertz radiation, Rep. Prog. Phys. **70**, 1325–1379 (2007).

[2] H. B. Liu, H. Zhong, N. Karpowicz, Y. Chen, and X.-C. Zhang, Terahertz spectroscopy and imaging for defence and security applications, Proc. IEEE **95**, 1514–1527 (2007).

[3] J. Chen, Y. Chen, H. Zhao, G. J. Basiaans, and X.-C. Zhang, Absorption coefficients of selected explosives and related compounds in the range of 0.1–2.8 THz, Opt. Express **15**, 12060–12067 (2007).

[4] A. Hirata, T. Kosugi, H. Takahashi, R. Yamaguchi, F. Nakajima, T. Furuta, H. Ito, H. Sugahara, Y. Sato, and T. Nagatsuma, 120-GHz-band millimeter-wave photonic wireless link for 10-Gb/s data transmission, IEEE Trans. Microwave Theory Tech. **54**, 1937–1944 (2006).

[5] R. Yamaguchi, A. Hirata, T. Kosugi, H. Takahashi, N. Kukutsu, T. Nagatsuma, Y. Kado, H. Ikegawa, H. Nishikawa, and T. Nakayama, 10-Gbit/s MMIC wireless link exceeding 800 meters, , in: Proceedings of the 2008 IEEE RWS, TH1C-3, Florida, 2008.

[6] R. Piesiewicz, T. Kleine-Ostmann, N. Krumbholz, D. Mittleman, M. Koch, J. Schoebel, and T. Kuerner, Short-range ultra-broadband terahertz communications: concept and perspectives, IEEE Antenna and Propagation Magazine **49**, 24–35 (2007).

[7] C. Mann, Practical challenges for the commercialization of terahertz electronics, , in: Proceedings of the IEEE/MTT-S International Microwave Symposium, Honolulu, 2007, pp. 1705–1708.

[8] M. Tonouchi, Cutting-edge terahertz technology, Nature Photonics **1**, 97–105 (2007).

[9] B. Shillue, S. Albanna, and L. D'Addario, Transmission of low phase noise, low phase drift millimeter-wavelength references by a stabilized fiber distribution system, Microwave Photonics, Tech. Digest, Ogunquit, USA (2004), pp. 201–204.

[10] T. Ishibashi, N. Shimizu, S. Kodama, H. Ito, T. Nagatsuma, and T. Furuta, Uni-traveling-carrier photodiodes, Ultrafast Electronics and Optoelectronics, Tech. Digest, Lake Tahoe, USA (1997), pp. 83–87.

[11] Z. F. Fan and N. Dagenais, Optical generation of a megahertz-linewidth microwave signal using semiconductor lasers and a discriminator-aided phase-locked loop, IEEE Trans. Microwave Theory and Tech. **45**, 1296–1300 (1997).

[12] L. A. Johansson and A. J. Seeds, Fiber-integrated heterodyne optical injection phase-lock loop for optical generation of millimeter-wave carriers, IEEE/MTT-S Intern. Microwave Symposium, Tech. Digest, Boston,USA (2000), pp. 1737–1740.

[13] D. Chen, H. R. Fetterman, A. Chen, W. H. Steier, L. R. Dalton, W. Wang, and Y. Shi, Demonstration of 110 GHz electro-optic polymer modulators, Appl. Phys. Lett. **70**, 3335–3337 (1997).

[14] K. Sato, 100 GHz optical pulse generation using Fabry-Perot laser under continuous wave operation, Electron. Lett. **37**, 763–764 (2001).

[15] T. Ohno, F. Nakajima, T. Furuta, and H. Ito, 240 GHz active mode locked laser diode, Electron. Lett. **41**, 1057–1059 (2005).

[16] A. Hirata, M. Harada, K. Sato, and T. Nagatsuma, Low-cost millimeter-wave photonic techniques for Gigabit/s wireless link, IEICE Trans. Electron. **E86-C**, 1123–1128 (2003).

[17] S. Fukushima, C. F. C. Silva, Y. Muramoto, and A. J. Seeds, Optoelectronic millimeter-wave synthesis using an optical frequency comb generator, optically injection locked lasers, and a unitraveling-carrier photodiode, IEEE J. Lightwave Technol. **21**, 3043–3051 (2003).

[18] M. Fujiwara, M. Teshima, J. Kani, H. Suzuki, N. Takachio, and K. Iwatsuki, Optical carrier supply module using flattened optical multicarrier generation based on sinusoidal amplitude and phase hybrid modulation, IEEE J. Lightwave Technol. **21**, 2705–2714 (2003).

[19] T. Yamamoto and S. Kawanishi, Generation of low-noise optical frequency comb and optical beat signal using phase modulator, Japan-Korea Workshop on Microwave and Millimeter-Wave Photonics, Tech. Digest, Otsu, Japan (2004), pp. 15–19.

[20] A. Hirata, H. Togo, N. Shimizu, H. Takahashi, K. Okamoto, and T. Nagatsuma, Low-phase noise photonic millimeter-wave generator using an AWG integrated with a 3-dB combiner, IEICE Trans. Electron. **E88-C**, 1458–1464 (2005).

[21] H.-J. Song, N. Shimizu, and T. Nagatsuma, Generation of two-mode optical signals with broadband frequency tunability and low spurious signal level, Opt. Express **15**, 14901–14906 (2007).

[22] C. F. C. Silva, A. J. Seeds, and P. J. Williams, Terahertz span $>$ 60-channel exact frequency dense WDM source using comb generation and SG-DBR injection-locked laser filtering, IEEE Photon. Technol. Lett. **13**, 370–372 (2001).

[23] C. C. Renaud, C. F. C. Silva, M. Dueser, P. Bayvel, and A. J. Seeds, Exact, agile, optical frequency synthesis using an optical comb generator and optical injection phase lock loop, 2003 IEEE LEOS Summer Topical Meetings WC1.3, Tech. Digest, Vancouver, Canada (2003), pp. 67–68.

[24] P. Shen, N. J. Gomes, P. A. Davies, P. G. Huggard, and B. N. Ellison, Analysis and demonstration of a fast tunable fibre-ring-based optical frequency comb generator, IEEE J. Lightwave Technol. **25**, 3257–3264 (2007).
[25] R. P. Scott, N. K. Fontaine, J. P. Heritage, B. H. Kolner, and S. J. B. Yoo, 3.5-THz wide, 175 mode optical comb source, IEEE/OSA Optical Fiber Communication Conference, Tech. Digest, OWJ3, San Diego, USA (2007).
[26] M. Sugiyama, Broadband $LiNbO_3$ modulators, Microwave Photonics, Tech. Digest, Ogunquit, USA (2004), pp. 273–276.
[27] H.-J. Song, N. Shimizu, T. Furuta, K. Suizu, H. Ito, and T. Nagatsuma, Broadband-frequency-tunable sub-terahertz wave generation using an optical comb signal, AWGs, optical switches, and uni-travelling carrier photodiode for spectroscopic applications, IEEE J. Lightwave Technol., to be published.
[28] T. Ishibashi, T. Furuta, H. Fushimi, S. Kodama, H. Ito, T. Nagatsuma, N. Shimizu, and Y. Miyamoto, InP/InGaAs uni-traveling-carrier photodiodes, IEICE Trans. Electron. **E83-C**, 938–949 (2000).
[29] H. Ito, S. Kodama, Y. Muramoto, T. Furuta, T. Nagatsuma, and T. Ishibashi, High-speed and high-output InP-InGaAs unitraveling-carrier photodiodes, IEEE J. Selected Topics in Quantum Electronics **10**, 709–727 (2004).
[30] H. Ito, T. Furuta, S. Kodama, and T. Ishibashi, InP/InGaAs uni-travelling-carrier photodiode with a 310 GHz bandwidth, Electron. Lett. **36**, 1809–1810 (2000).
[31] H. Ito, T. Furuta, F. Nakajima, K. Yoshino, and T. Ishibashi, Photonic generation of continuous THz wave using uni-traveling-carrier photodiode, IEEE J. Lightwave Technol. **23**, 4016–4021 (2005).
[32] G. A. Davis, R. E. Weiss, R. A. LaRue, K. J. Williams, and R. D. Esman, 920–1650 nm high current photodetector, IEEE Photon. Technol. Lett. **8**, 1373–1375 (1996).
[33] K. Kato, Ultrawide-band/high-frequency photodetectors, IEEE Trans. Microwave Theory Tech. **47**, 1265–1281 (1999).
[34] H. Fukano, A. Kozen, K. Kato, and O. Nakajima, Edge-illuminated refracting-facet photodiode with high responsivity and low-operation voltage, Electron. Lett. **32**, 2346–2347 (1996).
[35] K. Kato, A. Kozen, Y. Muramoto, Y. Itaya, T. Nagatsuma, and M. Yaita, 110-GHz, 50% efficiency mushroom-mesa waveguide p-i-n photodiode for a 1.55-μm wavelength, IEEE Photon. Technol. Lett. **6**, 719–721 (1994).
[36] G. Unterbörsch, A. Umbach, D. Trommer, and G. G. Mekonnen, 70 GHz long wavelength photodetector, in: Proceedings of the ECOC'97, Edinburgh, UK, 1997, Vol. 2, pp. 25–28.
[37] K. S. Giboney, M. J. W. Rodwell, and J. E. Bowers, Traveling-wave photodetector theory, IEEE Trans. Microwave Theory Tech. **45**, 1310–1319 (1997).
[38] A. Stöhr, R. Heinzekmann, C. Kaczmarek, and D. Jäger, Ultra-broadband Ka- to W-band 1.55-μm travelling-wave photomixers, Electron. Lett. **36**, 970–971 (2000).
[39] T. Chau, N. Kaneda, T. Jung, A. Rollinger, S. Mathai, Y. Qian, T. Itoh, M. C. Wu, W. P. Shillue, and J. M. Payne, Generation of millimeter waves by photomixing at 1.55 μm using InGaAs-InAlAs-InP velocity matched distributed photodetectors, IEEE Photon. Technol. Lett. **12**, 1055–1057 (2000).
[40] H. Fukano, Y. Muramoto, K. Takahata, and Y. Matsuoka, High efficiency edge illuminated uni-traveling-carrier structure refracting-facet photodiode, Electron. Lett. **35**, 1664–1665 (1999).
[41] Y. Muramoto, K. Kato, M. Mitsuhara, O. Nakajima, Y. Matsuoka, N. Shimizu, and T. Ishibashi, High-output-voltage, high speed, high efficiency uni-traveling-carrier waveguide photodiode, Electron. Lett. **34**, 122–123 (1998).
[42] Y. Hirota and T. Ishibashi, and H. Ito, 1.55-μm wavelength periodic traveling-wave photodetector fabricated using uni-traveling-carrier photodiode structures, IEEE J. Lightwave Technol. **19**, 1751–1758 (2001).
[43] M. Achouche, V. Magnin, J. Harari, F. Lelarge, E. Derouin, C. Jany, D. Carpentier, F. Blache, and D. Decoster, High performance evanescent edge coupled waveguide unitraveling-carrier photodiodes for $>$ 40-Gb/s optical receivers, IEEE Photon. Technol. Lett. **16**, 584–587 (2004).
[44] C. C. Renaud, M. Robertson, D. Rogers, R. Firth, P. J. Cannard, R. Moore, and A. J. Seeds, A high responsivity, broadband waveguide uni-travelling carrier photodiode (Photonics Europe 2006), Proc. SPIE **6194**, 61940C (2006).
[45] A. Madjar, N. Koka, J. Bloch, M. Draa, and P. K. L. Yu, A novel analytical model for the UTC-TW photodetector for generation of sub-mm wave signals, , in: Proceedings of the European Microwave Conference (EuMC), 2007, pp. 618–621.
[46] H. Ito, T. Nagatsuma, A. Hirata, T. Minotani, A. Sasaki, Y. Hirota, and T. Ishibashi, "High-power photonic millimetre wave generation at 100 GHz using matching-circuit-integrated uni-travelling-carrier photodiodes, IEE Proc. Optoelectron. **150**, 138–142 (2003).
[47] H. Ito, T. Furuta, Y. Muramoto, T. Ito, and T. Ishibashi, Photonic millimetre- and sub-millimetre-wave generation using J-band rectangular-waveguide-output uni-traveling-carrier photodiode module, Electron. Lett. **42**, 1424–1425 (2006).
[48] A. Hirata, T. Nagatsuma, R. Yano, H. Ito, T. Furuta, Y. Hirota, T. Ishibashi, H. Matsuo, A. Ueda, T. Noguchi, Y. Sekimoto, M. Ishiguro, and S. Matsuura, Output power measurement of photonic millimeter-wave and sub-millimeter-wave emitter at 100–800 GHz, Electron. Lett. **38**, 989–800 (2002).
[49] F. Nakajima, T. Furuta, and H. Ito, High-power continuous-terahertz-wave generation using resonant-antenna-integrated uni-traveling-carrier photodiode, Electron. Lett. **40**, 1297–1299 (2004).
[50] N. Shimizu and T. Nagatsuma, Photodiode-integrated microstrip antenna array for subterahertz radiation, IEEE Photon. Technol. Lett. **18**, 743–745 (2006).
[51] K. J. Williams, D. A. Tulchinsky, and J. C. Campbell, High-power photodiodes, Microwave Photonics, Tech. Digest, Victoria, Canada (2007), pp. 9–13.
[52] T. Nagatsuma, H. Ito, and T. Ishibashi, Photonic THz sources using uni-traveling-carrier photodiode technologies, IEEE LEOS Annual Meeting, Tech. Digest, ThN3, Florida, (2007), pp. 792–793.
[53] X. Li, N. Li, S. Demiguel, X. Zheng, J. C. Campbell, H. H. Tan, and C. Jagadish, A partially depleted absorber photodide with graded doping injection regions, IEEE Photon. Technol. Lett. **16**, 2326–2328 (2004).

[54] Y. Muramoto and T. Ishibashi, InP/InGaAs pin photodiode structure maximizing bandwidth and efficiency, Electron. Lett. **39**, 1749–1750 (2003).
[55] X. Li, S. Demiguel, N. Li, J. C. Campbell, D. L. Tulchinsky, and K. J. Williams, Backside illuminated high saturation current partially depleted absorber photodetectors, Electron. Lett. **39**, 1466–1467 (2003).
[56] Y.-S. Wu, J.-W. Shi, J.-Y. Wu, F.-H. Huang, Y.-J. Chan, Y.-L. Huang, and R. Xuan, High-performance evanescently edge coupled photodiodes with partially p-doped photoabsorption layer at 1.55-mm wavelength, IEEE Photon. Technol. Lett. **17**, 878–880 (2005).
[57] K. J. Williams, Comparison between dual-depletion-region and uni-travelling-carrier p-i-n photodetectors, IEE Proc. Optoelectron. **149**, 131–137 (2002).
[58] A. Joshi and D. Becker, GRIN lens-coupled top-illuminated photodetectors for high-power applications, Microwave Photonics, Tech. Digest, Victoria, Canada (2007), pp. 18–20.
[59] D.-H. Jun, J.-H. Jang, I. Adesida, and J.-I. Song, Improved efficiency-bandwidth product of modified uni-traveling-carrier photodiode structure using an undoped photoabsorption layer, Jpn. J. Appl. Phys. **45**, 3475–3478 (2006).
[60] J.-W. Shi, Y.-S. Wu, C.-Y. Wu, P.-H. Chiu, and C.-C. Hong, High-speed, high-responsivity, and high-power performance of near-ballistic uni-traveling-carrier photodiode at 1.55-mm wavelength, IEEE Photon. Technol. Lett. **17**, 1929–1931 (2005).
[61] Y.-S. Wu, J.-W. Shi, and P.-H. Chiu, Analytical modeling of a high-performance near-ballistic uni-traveling-carrier photodiode at a 1.55-mm wavelength, IEEE Photon. Technol. Lett. **18**, 938–940 (2005).
[62] N. Li, X. Li, S. Demiguel, X. Zheng, J. C. Campbell, D. A. Tulchinsky, K. J. Williams, T. D. Isshiki, G. S. Kinsey, and R. Sudharsansan, High-saturation-current charge-compensated InGaAs/InP uni-traveling-carrier photodiode, IEEE Photon. Technol. Lett. **16**, 864–866 (2004).
[63] Y. Royter, T. Furuta, S. Kodama, N. Sahri, T. Nagatsuma, and T. Ishibashi, Integrated packaging of over 100 GHz bandwidth uni-traveling-carrier photodiodes, IEEE Electron. Device Lett. **21**, 181–183 (2000).
[64] D. A. Tulchinsky, K. J. Williams, A. Pauchard, M. Bitter, Z. Pan, L. Hodge, S. G. Hummel, and Y. H. Lo, High-power InGaAs-on-Si pin RF photodiodes, Electron. Lett. **39**, 1084–1086 (2003).
[65] N. Li, H. Chen, N. Duan, M. Liu, S. Demiguel, R. Sidhu, A. L. Holmes, Jr., and J. C. Campbell, High power photodiode wafer bonded to Si using Au with improved responsivity and output power, IEEE Photon. Technol. Lett. **18**, 2526–2528 (2006).
[66] K. Yoshino, Y. Muramoto, T. Furuta, and H. Ito, High-speed uni-travelling-carrier photodiode module for ultra-low temperature operation, Electron. Lett. **41**, 1030–1031 (2005).
[67] H. Ito, T. Furuta, S. Kodama, K. Yoshino, T. Nagatsuma, and Z. Wang, 10-Gbit/s operation of a uni-travelling-carrier photodiode module at 2.6 K, Electron. Lett. **44**, 149–150 (2008).
[68] T. Furuta, T. Ito, Y. Muramoto, H. Ito, M. Tokumitsu, and T. Ishibashi, D-band rectangular-waveguide-output uni-travelling-carrier photodiode module, Electron. Lett. **41**, 715–716 (2005).
[69] Y. Sekimoto, A. Ueda, T. Okuda, E. Bryerton, M. Sugimoto, H. Matsuo, S. Yokogawa, T. Noguchi, M. Ishiguro, H. Ito, T. Nagatsuma, A. Hirata, and J. M. Payne, Noise evaluation of hybrid photonic local oscillators at 500 GHz, ALMA memo 449, March 20, 2003.
[70] A. Hirata, M. Harada, and T. Nagatsuma, 120-GHz wireless link using photonic techniques for generation, modulation, and emission of millimeter-wave signals, IEEE J. Lightwave Technol. **21**, 2145–2153(2003).
[71] H. Ito, T. Furuta, T. Kosugi, A. Hirata, H. Takahashi, Y. Muramoto, M. Tokumitsu, Y. Sato, T. Nagatsuma, and T. Ishibashi, "Over-10-dBm output uni-traveling-carrier photodiode module integrating a power amplifier for wireless transmissions in the 125-GHz Band, IEICE Electronics Express **2**, 446–450 (2005).
[72] H. Suzuki, M. Fujiwara, K. Iwatsuki, A. Hirata, and T. Nagatsuma, Photonic millimetre-wave generator using intensity and phase modulators for 10 Gbit/s wireless link, Electron. Lett. **41**, 355–356 (2005).
[73] R. W. Ridgway and D. W. Nippa, Generation and modulation of a 94-GHz signal using electrooptic modulators, IEEE Photon. Technol. Lett. **20**, 653–655 (2008).
[74] H. Ito, F. Nakajima, T. Ohno, T. Furuta, T. Nagatsuma, and T. Ishibashi, InP-based planar-antenna-integrated Schottky-barrier diode for a millimeter-and sub-millimeter-wave detection, Jpn. J. Appl. Phys., to be published.
[75] S. Takano, A. Ueda, T. Yamamoto, S. Asayama, Y. Sekimoto, T. Noguchi, M. Ishiguro, H. Takara, S. Kawanishi, H. Ito, A. Hirata, and T. Nagatsuma, The first radioastronomical observation with photonic local oscillator, Publ. Astron. Soc. Japan **55**, L53–L56 (2003).
[76] A. Stöhr, A. Malcoci, A. Sauerwald, I. C. Mayorga, R. Güsten, and D. Jäger, Ultra-wide-band traveling-wave photodetectors for photonic local oscillators, IEEE Technol. **21**, 3062–3070 (2003).
[77] S. Kohjiro, Y. Uzawa, J. Inatani, T. Nagatsuma, H. Ito, Z. Wang, and A. Shoji, Quasi-optical superconducting heterodyne receiver using a photonic local oscillator in the submillimeter-wave region, of the International Workshop on Terahertz Technology, Tech. Digest, 18B-6, Osaka, 119–120 (2005).
[78] H.-J. Song, N. Shimizu, T. Furuta, K. Suizu, H. Ito, and T. Nagatsuma, Broadband frequency tunable photonic subterahertz wave generation for spectroscopic applications, Tech. Digest, 20th Annual Meeting of the IEEE Lasers and Electro-Optics Society, ThF2, 733–734 (2007).
[79] HITRAN homepage, http://cfa-www.harvard.edu/hitran/welcometop.html.
[80] J. R. Demers, R. T. Logan Jr., and E. R. Brown, An optically integrated coherent frequency-domain THz spectrometer with signal-to-noise ratio up to 80 dB, Microwave Photonics, Tech. Digest, Victoria, Canada (2007), pp. 92–95.
[81] M. N. Feiginov, Analysis and limitations of terahertz p-i-n uni-traveling-carrier photodiodes, J. Appl. Phys. **102**, 084510 (2007).